DOI: 10.24352/UB.OVGU-2017-080 TECHNISCHE MECHANIK, 37, 1, (2017), 37 – 47
submitted: July 6, 2017

Numerical Investigation of the Phase Evolution in Polymer Blends under External Mechanical Loadings

J. Voges, R. Makvandi, D. Juhre

The influences on the development of polymer blend microstructures are not yet fully understood in the manufacturing processes. The purpose of this paper is to give a closer look at the effect of the elastic energy on the decomposition process. The decomposition process of a melt consisting of two polymers with different shear moduli is investigated. Due to the resulting heterogeneous material behavior and deformations, the generated energy field is heterogeneous as well. This energy causes changes in the local stability of the mixture, which yields phases consisting of both the polymers. Additionally, possible large deformations result in dominating diffusion directions.

1 Introduction

In the manufacturing process, the microstructure of polymer blends strongly depends on different effects. To better control the resulting microstructures, it is important to know the behavior of these single effects. One method to mix polymers is to stir the melt, which causes an elastic deformation besides the mixing. A numerical simulation can give some preliminary information on the influences on the phase behavior. A useful method for this is the phase-field method. Here, an order parameter which is defined on the whole domain denotes the present phase and thus the present material at any point of the domain. There is no need to track the phases boundaries. There are different approaches for phase-field models. A large part is based on the Cahn-Hilliard equation. The theoretical framework for this differential equation (DE) is provided by John W. Cahn and John E. Hilliard (see Cahn and Hilliard (1957), Cahn and Hilliard (1959) and Cahn and Hilliard (1961)). Using this equation, the evolution of the order parameter can be described (cf. e. g. Zhu et al. (2016)).

Studying the evolution of phases in the presence of external mechanical loadings can help to understand material behaviors in a better way. To investigate this numerically, the Cahn-Hilliard equation can be coupled with elasticity. One popular method among researchers is based on adding an elastic energy to the free energy of the system. The elastic energy contains material parameters which may depend on the order parameter. Based on this, Yeon et al. (2005) simulated the anisotropic dendritic growth due to elastic stresses in a binary alloy. Ubachs et al. (2004) investigated the phase evolution of tin-lead solder under global strain and considered small deformations in one-dimensional simulations with phase dependent material parameters likewise. By applying a global strain, they observed that the concentrations in the phases change respectively. Another way of coupling based on the elastic energy is to model the swelling due to a phase change. The basic framework for this is developed by Anand and Chester (2010) and Duda et al. (2010), which both hold for large deformations. They also discussed that there are two different possibilities to formulate the Cahn-Hilliard equation. One must choose between the material description and the spatial description to derive the governing equations, which correlates with a deformation independent and dependent diffusion, respectively. Hong and Wang (2013) implemented an algorithm to model the swelling of polymeric gels. A swelling due to the lithiation of electrode materials is discussed by Di Leo et al. (2014) and Zao et al. (2016), who also formulated phase dependent values for the material parameters. In both the papers, however, the deformation dependent diffusion is not studied. In the manufacturing process, laminar phases, which are due to shear flows, can often be observed (cf. Han et al. (2006) and Liu et al. (2013)). The viscoplastic behavior of solder alloys based on a phase-field is investigated by Ubachs et al. (2005). The diffusion in a decomposition process does not need to be isotropic. Kuhl and Schmid (2007) show an implementation of the anisotropic Cahn-Hilliard equation.

In regard to numerics, there are different approaches for the local discretization of the Cahn-Hilliard equation. The Finite Difference Method (FDM), because of the simplicity of its implementation, is usually the most convenient

method to consider (cf. e. g. Lee et al. (2014) and Ju et al. (2015)). However, when dealing with mechanical couplings and complex geometries, other numerical methods like the finite element method (FEM) seem to be an inevitable choice. Since the Cahn-Hilliard equation is a fourth-order differential equation and needs C^1-continuous elements (with continuous first derivative across the elements), the conventional finite element method with mostly Lagrangian interpolation functions (which can only provide C^0-continuity across elements) is not able to solve the problem, therefore some approaches to overcome this issue have been proposed. One way of doing this, is to split the fourth-order governing equation into two coupled second-order equations. Another approach is to change the discretization technique itself. For instance, the discontinuous Galerkin method can be used (cf. Wells et al. (2006)). In Kaessmair and Steinmann (2016) it is shown that the isogeometric analysis (IGA) provides a good numerical performance for phase-field models by comparing different numerical methods. Detailed convergence studies are done by Gómez et al. (2008) and Kästner et al. (2016) as well. Based on this, in the present work the method of choice is the IGA. The finite element software FEAP with an IGA extension is used (nurbFEAP) (cf. Taylor (2014)). The software nurbFEAP provides an IGA framework based on the Bézier extraction method (cf. Borden et al. (2011)).

A mixture with unstable volume fractions of its components yields a spontaneous decomposition. While decomposing, in any part of the mixture there is a specific concentration of the materials. Concentrations, which behave stable, are referred to as concentrations *in the stable domain* or *in the stable concentration intervals* in this paper. This holds for metastable and unstable conditions in a same way. The purpose of this work is to illustrate changes of the stabilities boundaries due to external loads within a two-dimensional domain and finite elasticity (large deformations theory of elasticity). Phase dependent material parameters are applied.

The next chapter will be about the mathematical derivation of the governing equations. Here, the phase-field method is introduced in detail and the elasticity is elaborated. Chapter 3 deals with the numerics and the presentation of the residual formulation for the IGA framework. Chapter 4 is divided into two considerations. First, kinematical effects due to the large deformations are studied, and second, the shift of the stabilities is investigated. The last chapter provides a conclusion.

2 Model

This section deals with the derivation of the governing differential equations. A coupling between the phase-field model and the finite deformations elasticity theory is established. There are dependencies in both directions: The mixing energy in the phase-field is influenced by the resulting elastic energy and the elastic material parameters are dependent on the phase-field.

2.1 Phase-field method

Assume a binary mixture with A and B as its components. Let $\{c \in \mathbb{R} \mid 0 \leq c_B \leq 1\}$ be an order parameter representing the volumetric concentration of component B, the concentration of component A will be $c_A = 1 - c_B$. For brevity $c = c_B$ holds. In a two dimensional domain $\mathcal{B} \subset \mathbb{R}^2$ the order parameter is defined for every spatial point $\mathbf{x} \in \mathcal{B}$.

Assuming a transient problem, the diffusion equation is described by

$$\frac{\partial c}{\partial t} = -\operatorname{div} \mathbf{j} \qquad \text{with} \qquad \mathbf{j} = -\mathbf{M} \nabla \mu, \tag{1}$$

where $\mathbf{j}$ denotes the concentration flux and is based on the chemical potential μ and the mobility tensor $\mathbf{M}$. In the special case of isotropic diffusion, the mobility tensor becomes $\mathbf{M} = M\mathbf{1}$ with the degenerative mobility M, which is a function of the concentration and in this paper is calculated using the following equation.

$$M(c) = D(1 - c)c, \tag{2}$$

where D is the diffusive coefficient and is constant. Let ψ be the volume-specific free energy of the system, the chemical potential is defined by the variational derivative with respect to c:

$$\mu = \frac{\delta\psi}{\delta c} = \frac{\partial\psi}{\partial c} - \operatorname{div}\frac{\partial\psi}{\partial\nabla c} \qquad \text{with} \qquad \psi(c,\nabla c) = \psi_{mi}(c) + \psi_{el}(c) + \psi_{in}(\nabla c). \tag{3}$$

According to the work of Cahn and Hilliard (1957), the interface energy is $\psi_{in} = \frac{1}{2}\lambda\nabla c \cdot \nabla c$ with a constant λ, hence the divergence term in equation (3) becomes

$$\operatorname{div}\frac{\partial\psi}{\partial\nabla c} = \frac{1}{2}\lambda\,\nabla\cdot\frac{\partial(\nabla c\cdot\nabla c)}{\partial\nabla c} = \lambda\,\nabla^2 c \qquad \text{and thus} \qquad \mu = \psi'_{mi}(c) + \psi'_{el}(c) - \lambda\nabla^2 c. \tag{4}$$

Here, the apostrophe denotes the first derivative with respect to c. The mixing energy ψ_{mi} reads

$$\frac{v_{mol}\;\psi_{mi}(c)}{N_a k_b T} = c\;\ln c + (1-c)\;\ln(1-c) + \omega c(1-c) \tag{5}$$

and is used in an analogous representation in Cahn and Hilliard (1957) and is a well-known equation in the Flory-Huggins solution theory. In equation (5) N_a is the Avogadro constant, k_b is the Boltzmann constant and T denotes the Kelvin temperature. In the present work, the mixing behavior due to the mixing energy is symmetric: both the polymers have the same tendency to be dissolved in the other polymer. Therefore, the molar volume v_{mol} is the same for both the polymers. This yields $v_{mol} = N_A v_A = N_B v_B$ with the degrees of polymerization N_i and the molar volumes of the corresponding monomers, v_i. The parameter ω corresponds to the interactions of the mixture and yields the typical double-well shape in Figure 1b.

Originated in the theoretical framework, which Gibbs provided in the 19th century, the stability of mixtures behaves as follows. Cahn and Hilliard (1959) picked up the idea that if $\partial^2 f/\partial c^2 < 0$, a spontaneous decomposition will occur. Here f represents the free energy without the interface energy, $f(c) = \psi_{mi}(c) + \psi_{el}(c)$. This yields the *spinodal points*, c_s, at $\partial^2 f/\partial c^2 = 0$, which thus delimit the left and the right border of the unstable domain.

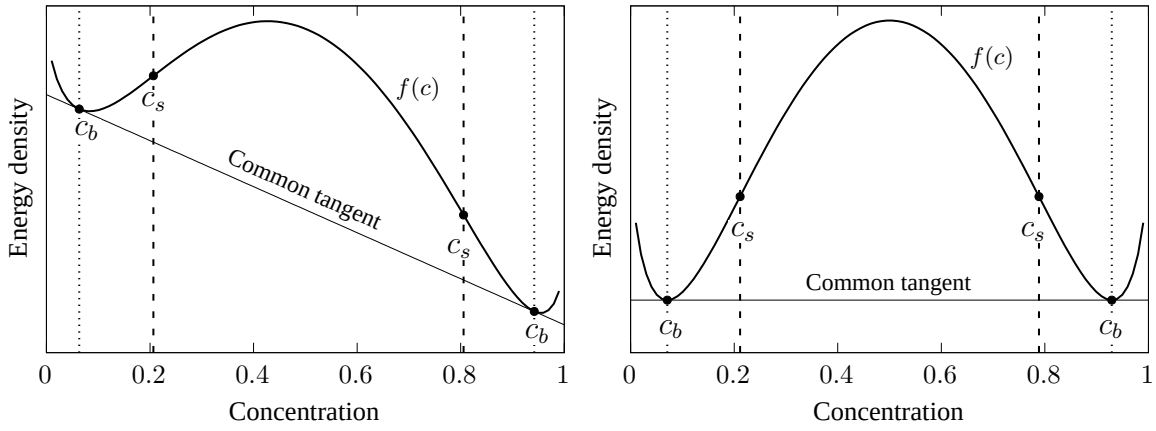

(a) General case

(b) Symmetric case, $\psi_{mi}(c)$

Figure 1. Energy function $f(c)$, corresponding spinodal points, c_s, and binodal points, c_b

The plot in Figure 1a shows a more general case of a mixing potential (cf. Cahn and Hilliard (1957)). The common tangent defines the borders between the metastable and the stable domains. A very detailed presentation of this correlation is provided by Wasylkiewicz et al. (1996) and also Baker et al. (1982). The two points corresponding to the common tangent are called *binodal points*, c_b.

In the classical theory the mixing energy and the interface energy are considered. Later the elastic energy is added (cf. e. g. Asaro and Tiller (1972)). In the isotropic case, the Cahn-Hilliard equation then becomes

$$\frac{\partial c}{\partial t} = \operatorname{div}\left[M(c)\,\nabla\big(f'(c) - \lambda\,\nabla^2 c\big)\right]. \tag{6}$$

Multiplying equation (6) with a scalar-valued test function, w, integrating over the domain $\mathcal{B}$ and applying the divergence theorem yields

$$\begin{aligned}\int_{\mathcal{B}} \left(\frac{\partial c}{\partial t} w + M(c)\; f''(c)\;\nabla c \cdot \nabla w + \lambda \nabla^2 c\; M'(c)\;\nabla c \cdot \nabla w + \lambda \nabla^2 c\; M(c)\;\nabla^2 w\right)\; dv \\ = \int_{\partial\mathcal{B}} M(c) \nabla\left(f'(c) - \lambda \nabla^2 c\right) \cdot \mathbf{n}\; w\; da + \int_{\partial\mathcal{B}} M(c) \lambda \nabla^2 c\; \nabla w \cdot \mathbf{n}\; da.\end{aligned} \tag{7}$$

Equation (7) is well-known and can be found in an analogous formulation in Kästner et al. (2016) and Kaessmair and Steinmann (2016). Here $\mathbf{n}$ denotes a normal vector belonging to the surface. It is more convenient to apply homogeneous boundary conditions on the domain to eliminate the right-hand side of the weak form (cf. e. g. Kästner et al. (2016)).

2.2 Elastic Energy

The finite deformation framework is used. Some kinematical quantities can be derived from the deformation gradient, $\mathbf{F} = \frac{\partial x_i}{\partial X_j} \mathbf{e}_i \otimes \mathbf{e}_j$ for spatial points $\mathbf{x} = x_i \mathbf{e}_i$ and material points $\mathbf{X} = X_i \mathbf{e}_i$. Thus, $\mathbf{C} = \mathbf{F}^T \mathbf{F}$ and its trace $I_C = C_{ii}$ can be formulated. The determinant of $\mathbf{F}$ is called Jacobian, $J = \det \mathbf{F}$. Based on this an elastic energy function for a compressible neo-Hookean material can be formulated:

$$\psi_{el} = \left(K - \frac{2}{3} G\right) U + \frac{1}{2} G\,(I_C - 3 - 2 \ln J) \qquad \text{and} \qquad U = \frac{1}{4}(J^2 - 1 - 2\,\ln J) \tag{8}$$

with the bulk modulus K and the shear modulus G.

Since the binary mixture consists of two different materials (phases) and the order parameter c defines the local present material, the mechanical behavior is assumed to change depending on c. This idea is also proposed in Di Leo et al. (2014) and also in Yeon et al. (2005), where the following interpolation function is provided:

$$h(c) = c^3(6c^2 - 15c + 10) \tag{9}$$

with $h(0) = 0$ and $h(1) = 1$. The shear modulus can be determined using

$$G(c) = G_A h(1 - c) + G_B h(c). \tag{10}$$

Here, the indices A and B represent the corresponding material phases. The materials are assumed to have both the same behavior regarding bulk deformations, so K is set to be independent of c. Figure 2a shows the qualitative shape of the function in equation (10). The shear moduli are quite small, which is due to the usage of melts.

Considering a specific deformation yields with equation (8) an elastic energy, which depends on the order parameter c. Let the shear moduli satisfy $G_A > G_B$, the stored elastic energy of a deformed block consisting of 100% of material A, can be expected to be larger than the same energy of a block consisting of 100% of material B with the same forced deformation. This effect is represented in Figure 2b. The concentration dependent elastic energy of a specific deformation state, which occurs in later considerations, is illustrated. Since the elastic energy is linear with respect to G, the shear modulus and the elastic energy look the same in their qualitative shape. The

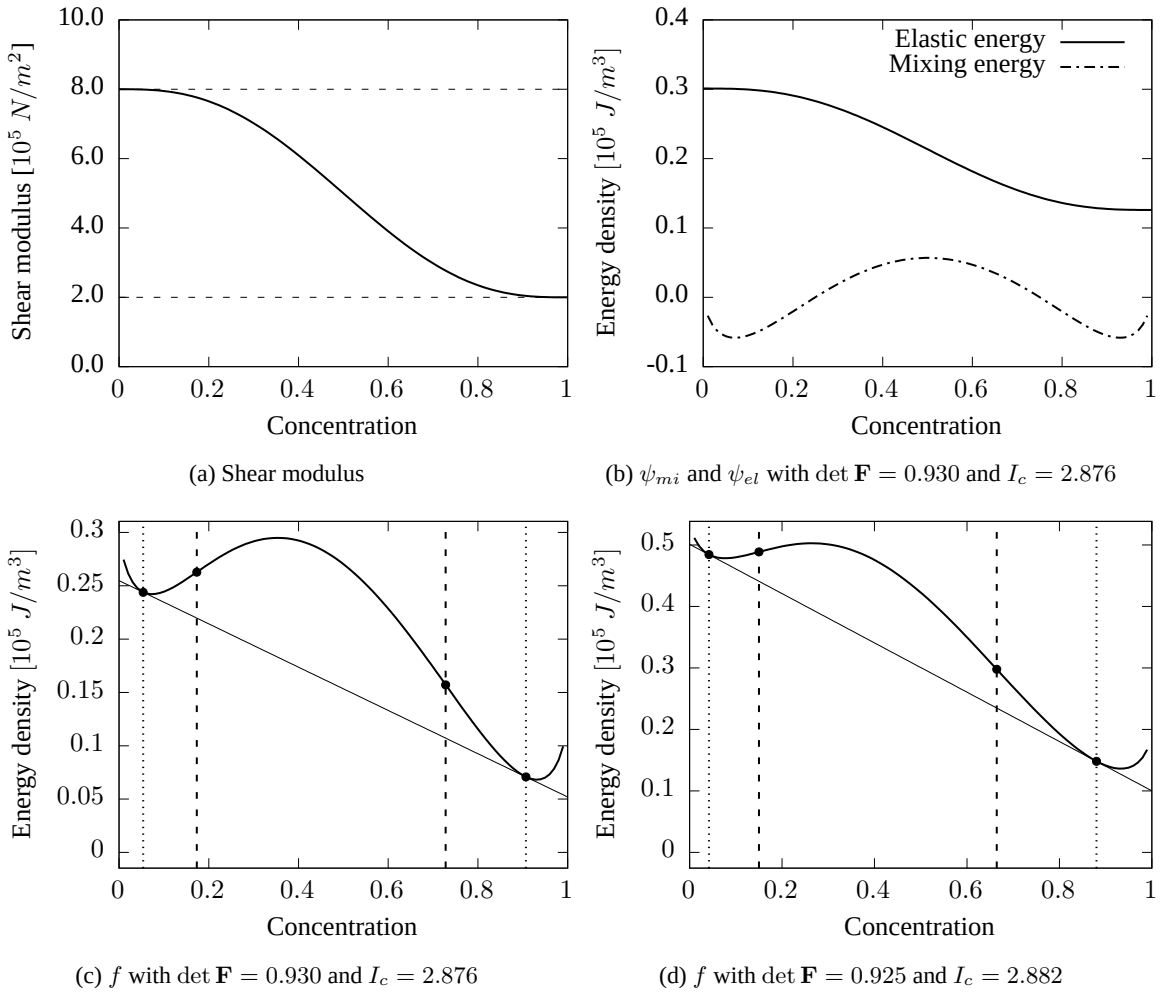

(a) Shear modulus

(b) ψ_{mi} and ψ_{el} with $\det \mathbf{F} = 0.930$ and $I_c = 2.876$

(c) f with $\det \mathbf{F} = 0.930$ and $I_c = 2.876$

(d) f with $\det \mathbf{F} = 0.925$ and $I_c = 2.882$

Figure 2. Shear modulus and elastic energy depending on the concentration; shift of the binodal and the spinodal points in $f(c)$ due to elastic deformations of different degrees

double-well potential ψ_{mi} is shown as well. Following the approach for $f(c)$ by summing up ψ_{el} and ψ_{mi}, the graph in Figure 2c results. A slightly different deformation yields the graph in Figure 2d. The binodal points and the spinodal points are shifted.

In order to apply actual deformations on a domain $\mathcal{B}$ to cause an elastic energy field, the following equations and quantities are used. The balance of linear momentum, also known as Cauchy's first law of motion, reads

$$\operatorname{div} \boldsymbol{\sigma} + \rho(\mathbf{b} - \mathbf{a}) = 0 \tag{11}$$

with the mass density ρ, the body force density $\mathbf{b}$ and the acceleration $\mathbf{a}$. The tensor $\boldsymbol{\sigma} = J^{-1}\mathbf{F}\mathbf{S}\mathbf{F}^T$ is the Cauchy stress tensor, where $\mathbf{S}$ is the second Piola-Kirchhoff stress tensor, $\mathbf{S} = 2\frac{\partial \psi}{\partial \mathbf{C}}$. Considering a quasi-static case and neglecting any body forces, equation (11) reduces to

$$\operatorname{div} \boldsymbol{\sigma} = 0. \tag{12}$$

Introducing a vector-valued test function $\mathbf{w}$, the weak form for the elastic part becomes

$$\int_{\mathcal{B}} \boldsymbol{\sigma} \cdot (\mathbf{w} \otimes \nabla)\, dv - \int_{\partial \mathcal{B}_\sigma} \mathbf{w} \cdot \mathbf{t}\, da = 0, \tag{13}$$

where $\mathbf{t}$ is the stress vector on a surface with normal direction $\mathbf{n}$. In later considerations the second term of equation (13) vanishes since the boundary conditions regarding surface stresses are chosen to be homogeneous.

3 Numerics

The Cahn-Hilliard equation and Cauchy's first law of motion yield a system of nonlinear partial differential equations. To solve these equations, a spatial and temporal discretization and a solution algorithm for non-linear problems are used. The governing equations are discretized using the NURBS based isogeometric analysis. The IGA allows higher continuities across element boundaries.

The spatial domain $\mathcal{B}$ is subdivided into n_e elements, which each are represented by the element domains, $\mathcal{B}_e$. As well-known from the finite element framework, the following residual equations can be derived for each control point, I, in spatial configuration

$$\bar{\mathbf{R}}_e^I = \int_{\mathcal{B}_e} (\mathbf{B}^I)^T \bar{\boldsymbol{\sigma}} dv = \int_{\mathcal{B}_e} \begin{bmatrix} N_{I,1} & 0 & N_{I,2} \\ 0 & N_{I,2} & N_{I,1} \end{bmatrix} \begin{bmatrix} \sigma_{11} \\ \sigma_{22} \\ \sigma_{12} \end{bmatrix} dv. \tag{14}$$

Here, N_I are the shape functions with $N_{I,i} = \partial N_I / \partial x_i$ for brevity. The vector $\bar{\boldsymbol{\sigma}}$ contains the independent entries of the second-order tensor $\boldsymbol{\sigma}$. Since the domain is $\mathbb{R}^2$ the nodal residual $\bar{\mathbf{R}}_e^I$ has one entry for each direction x_1 and x_2. In contrast, $\mathbf{R}_e^I$ has an additional entry for the nodal phase-field residual in the spatial configuration:

$$R_{e;P}^I = \int_{\mathcal{B}_e} \left(N_I \frac{\partial c}{\partial t} + M(c) f''(c) N_{I,i} c_{,i} + \lambda c_{,jj}\, M'(c) N_{I,i} c_{,i} + \lambda c_{,jj} M(c) N_{I,ii} \right) dv \tag{15}$$

where $R_{e;P}^I$ denotes the phase-field part of the residual. Indices appearing twice in a single term imply summation over the values 1 and 2 of the index, hence $c_{,ii}$ represents $\nabla^2 c$ in index notation. It should be noted that equation (15) can be found for example in Kästner et al. (2016) and Kaessmair and Steinmann (2016), who both do not include elastic couplings. The representation of this equation is not different from the literature, since the elastic coupling is realized by adding an additional term inside $f(c)$. The same holds for equation (14): The concentration dependency of the material moduli does not affect the derivation of the residual.

The time domain is discretized as well. For numerical integration a Newmark method is implemented in the solution algorithm of the Newton-Raphson method following Friberg (1987).

4 Behavior of the system

In all numerical examples, a two-dimensional square domain with the edge length $l_0 = 10\mu m$ is considered and an initial concentration field with $c = \bar{c} + c_n$ in every point is set. Here an average concentration $\bar{c} = 0.5$ is used, so both the components have the same volume fraction in the mixture. A small noise c_n with random values ensures that the right side of equation (6) does not vanish which otherwise would cause $\partial c / \partial t = 0$ in every point and thus the decomposition process would not start. Gómez et al. (2008) provide a mesh convergence study for the NURBS based IGA for the Cahn-Hilliard equation with the same double-well potential as in the present paper. Based on their findings, the mesh size is chosen to be 64×64 with cubic NURBS elements. In this choice, of course, the extension regarding the elasticity is taken into account as well. The influence on the error is expected to be small, an additional calculation using a mesh with 128×128 with cubic NURBS elements did not show notable differences. The edges of the two-dimensional domain have no-flux boundary conditions $\nabla c \cdot \mathbf{n} = 0$ (cf. Liu et al. (2013)). There are two general effects which can be observed. The first one is caused by the kinematics corresponding to the large deformations, and the other is coming from the elastic energy.

4.1 Kinematical effects

As already mentioned, Anand and Chester (2010) show that, when considering large deformations, one must choose between the material description and the spatial description to derive the governing equations. In the present work, deformation dependent diffusion is considered. This is assumed due to the consideration that in reality a particle tends more to attract the adjacent particles. This assumption yields either an anisotropic mobility tensor $\mathbf{M}_m$ in the material description or an isotropic mobility tensor $\mathbf{M}_s$ in the spatial description (cf. Hong and Wang (2013)). In the present paper, the spatial mobility tensor is applied.

To show the influence of the external loads on the diffusion directions, in this section three different kinds of boundary conditions are considered, which are shown in Figure 3. Note that all forced non-zero displacements are applied on the upper edge. In the simulations the displacements are $u_\alpha = 0.2l_0$ and $u_\beta = 0.3l_0$.

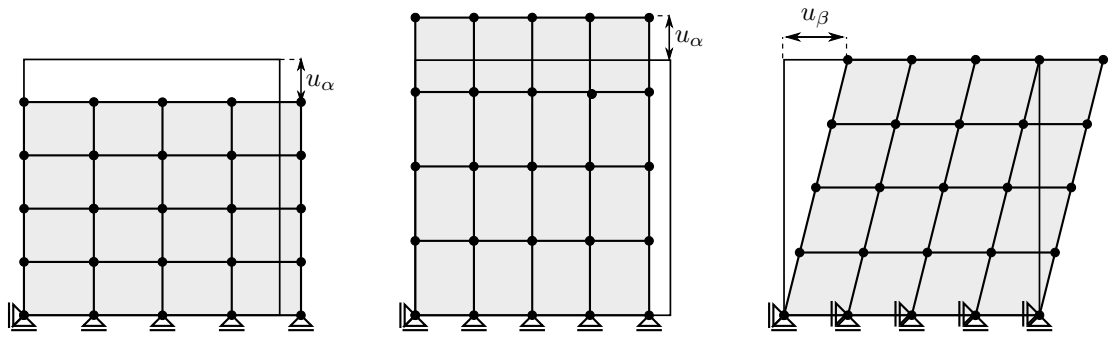

(a) Compression (b) Tension (c) Simple shear

Figure 3. Schematic representation of the considered deformations to investigate the kinematical effects

The deformation yields dominating diffusion directions which are due to the displacements of the nodes. The smaller the distance between the nodes the more those nodes are likely to create a common phase. This effect can be observed in Figure 4. Note that in contrast to Figure 4a, in Figure 4b the dominating direction corresponds with the direction of transversal contraction. The simple shear in Figure 4c yields a preferred diffusion direction, which is diagonal from top left to bottom right.

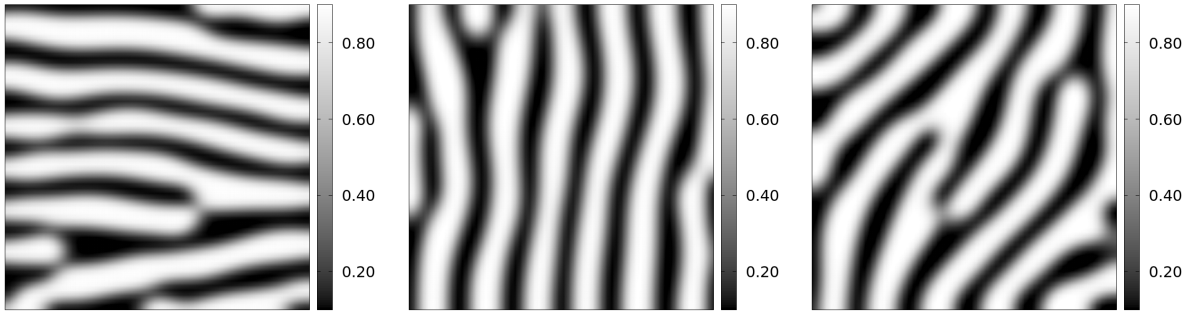

(a) Compression (b) Tension (c) Simple shear

Figure 4. Plot of the undeformed domain, showing the order parameter c at an equal simulation time

4.2 Energy based effects

In chapter 2.1, the binodal and the spinodal points are described. Figure 2 shows $f(c) = \psi_m + \psi_{el}$ for different applied deformations. As already mentioned, the inflection points represent the spinodal points and the common tangents define the binodal points of each curve. Due to the well-known fact that these points correlate with the stable, metastable and unstable concentrations of the components, it can be expected that the arising microstructure in a mechanical loaded state may differ from the one in an unloaded state.

The main question then becomes: how might these loads affect the decomposition? To get an idea of this, the following consideration has been made: A two-dimensional quadrilateral domain is deformed unevenly, cf. Figure

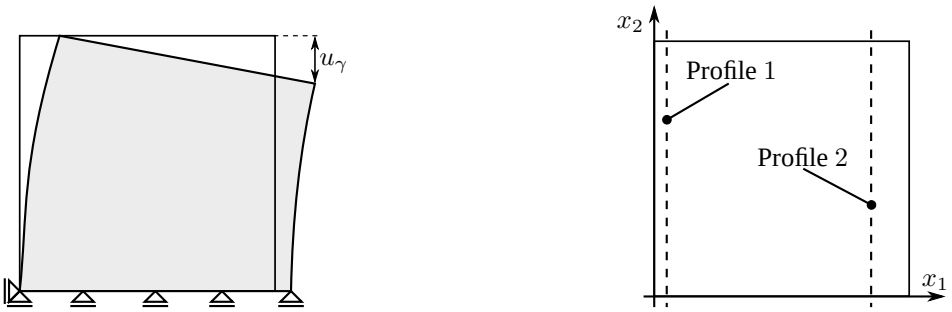

(a) Deformation (b) Marking for profile plots

Figure 5. Schematic representation of the considered deformation to investigate the effects in the fully coupled case; the vertical dashed lines mark the coordinates of profile plots in later considerations

5a. On the top edge, vertical boundary conditions are set following a linear function being dependent on the horizontal coordinate and having the maximum $u_\gamma = 0.15$. The bottom left corner is the only place where a horizontal displacement is inhibited. Note that this deformation, obviously, cannot be reproduced using polymer melts. However, to show the influence of the elastic energy, this consideration is sufficient.

Based on the mentioned boundary conditions, the quantities $\det \mathbf{F}$ and I_c can be assumed to be bigger on the right-hand side of the deformed domain. This yields a bigger elastic energy on the right-hand side, since equation (8) is dependent on these two kinematic quantities. Therefore, $\det \mathbf{F}$ and I_c can move the binodal and spinodal points (cf. Figure 2) and thus the borders of the stable and unstable concentration intervals, which influence the decomposition process of the binary mixture. Figure 6 b–c show the distribution of those quantities corresponding to the concentration field in Figure 6a. Note that the system is not in the equilibrium state.

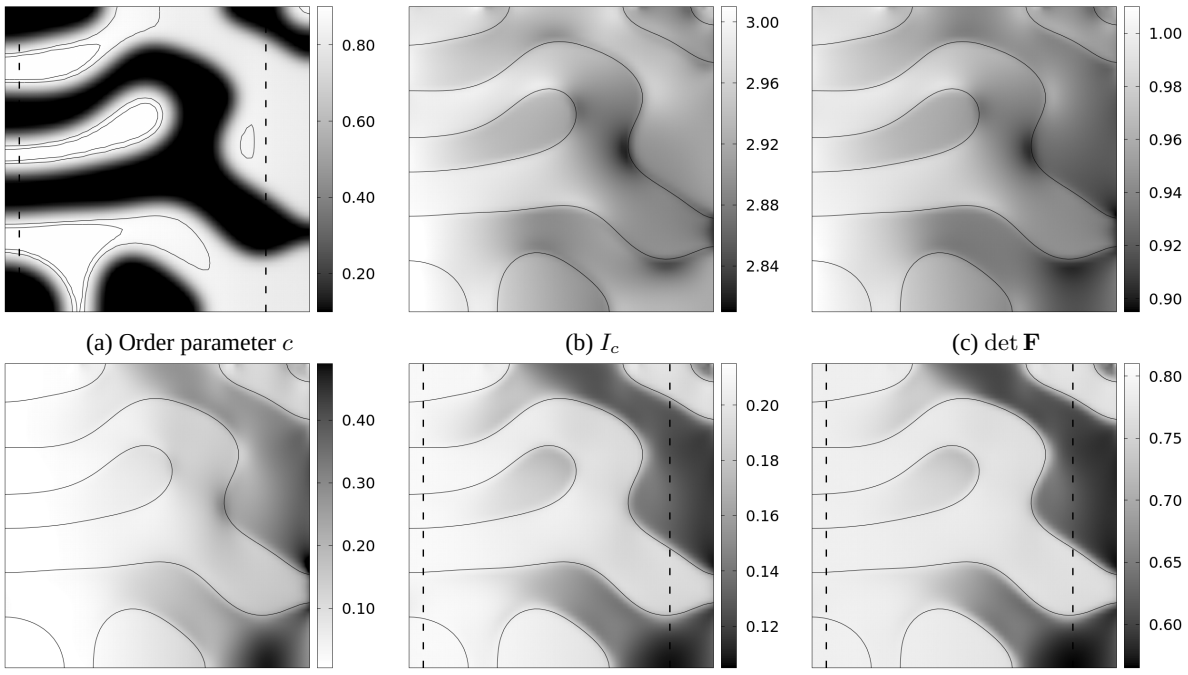

(a) Order parameter c (b) I_c (c) $\det \mathbf{F}$

(d) Elastic energy density $[10^5\ J/m^3]$ (e) First binodal point (f) Second binodal point

Figure 6. Quantities at an arbitrary simulation time; the dashed lines mark the coordinates of profile plots in later considerations; in (a), the contour lines represent $c = 0.85$ and $c = 0.90$, in (b)–(f), the contour lines represent $c = 0.5$

To illustrate changes in the borders of the stable concentration intervals, Figure 6 (e)–(f) provide the binodal points. Since in the considered cases the energy function has two binodal points (cf. Figure 1), there is one surface plot for each point. The stiffer phase is deformed less, so the binodal points do not change very much in the corresponding areas. The darker the color, the more the binodal point is changed in comparison to an undeformed system. The qualitative shape of the spinodal field behaves quite similar, so an illustration is dropped. However, these surface

plots serve just to get a first idea of the changes in the stability. The following consideration is more precise and includes the spinodal points as well.

For a closer look, Figure 7 represents profile plots corresponding to the dashed lines in Figure 5b and 6. The actual concentrations and the borders of stability based on the binodal points and the spinodal points are shown. Figure 7a represents a weakly deformed area. Here, unstable, metastable and stable concentration intervals are quite similar along the x_2-axis. Figure 7b, however, represents a strongly deformed area. Generally speaking, the actual concentrations tend to be at the binodal points and thus at the borders of the stable domain. It is a well-known fact that once the actual concentration reaches stability, a further decomposition cannot be expected, irrespective of the local minima in the energy function (cf. e. g. Kuhl and Schmid (2007)).

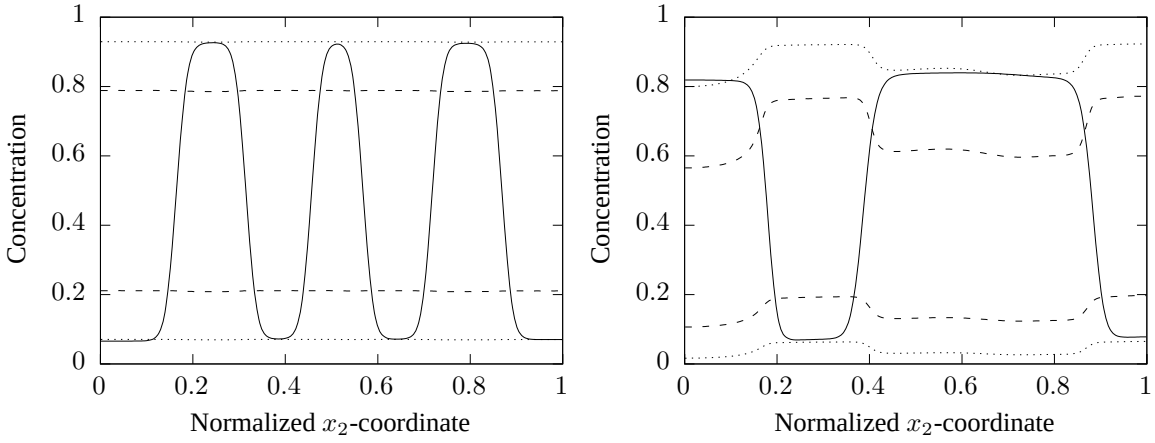

(a) Profile 1 (weakly deformed area)

(b) Profile 2 (strongly deformed area)

Figure 7. Profile plots, correspondng to the dashed lines in Figure 5b, 6a, 6e and 6f; actual concentration values (solid lines), spinodal points (roughly dashed lines) and binodal points (finely dashed lines)

While the stability border changes at $x_2 \approx 0.7$ in Figure 7b, the actual concentration behaves smoother, which is due to the surface energy term in equation (6), which forces the curvature to be low. The small deviation between stability border and the actual concentration at $x_2 \approx 0.1$ is assumed to be influenced by the same reason along with the no-flux boundary condition $\nabla c \cdot \mathbf{n} = 0$ at the edges, which forces the slope of the concentration curve in 7b to be zero at $x_2 = 0$ and $x_2 = 1$. It also matters that the solution is not in the equilibrium state, especially when considering the phases being in the metastable domain (e. g. at $x_2 \approx 0.3$).

Obviously, in Figure 7 the binodal points of the material having a smaller shear modulus tend to change more than the binodal points of the other material. This is due to the shape of the functions in Figure 2a and 2b. The stronger the deformation becomes, the more ψ_{el} dominates $f(c)$, thus ψ_{el} limits the shift of the binodal points being defined by the common tangent of $f(c)$ in each case.

5 Conclusions

The present work shows numerical studies providing two major effects caused by the presence of elastic energy and large deformations in a heterogeneous domain to investigate the phase behavior of polymer blends. First, the shift of the binodal points due to the energy, and second, the dominating diffusion directions caused by the deformations are investigated. This shift happens unevenly along the domain, since the energy field is heterogeneous. While the resulting diffusion directions occur regardless of the chosen materials, the shift of the binodal points requires two materials with different elastic moduli. The laminar structures due to preferred diffusion directions should not be confused with the laminar structures due to shear flows (cf. e. g. Han et al. (2006)). These two effects are due to different physical mechanisms and should not be confused. The effect in the present work is rate-independent. However, it can be assumed that both these mechanisms can occur at the same time in a shear flow, if deformation is permitted.

As already mentioned, the purpose of the proposed model is to give a first idea. However, the results permit the assumption that these effects may be observed in real experiments as well. In order to verify this assumption by comparing with experiments, the model must be improved by using a viscoelastic material model which considers

the relaxation of the mechanical energy, and considering non-static mechanical loads (e. g. forced strain rates) which counteract with the relaxation and thus, shift the binodal and the spinodal points. For instance, the strain rate could be chosen to fit those strain rates, which occur in the process of stirring a melt in the manufacturing process of polymer blends.

References

Anand, L.; Chester, S. A.: A coupled theory of fluid permeation and large deformations for elastomeric materials. *J. Mech. Phys. Solids*, 58, (2010), 1879 – 1906.

Asaro, R. J.; Tiller, W. A.: Interface morphology development during stress corrosion cracking: Part i. via surface diffusion. *Metall. Trans.*, 3, (1972), 1789 – 1796.

Baker, L. E.; Pierce, A. C.; Luks, K. D.: Gibbs energy analysis of phase equilibria. *Soc. Petrol. Eng. J.*, 22, (1982), 731 – 742.

Borden, M. J.; Scott, M. A.; Evans, J. A.; Hughes, T. J. R.: Isogeometric finite element data structures based on bzier extraction of nurbs. *Int. J. Numer. Meth. Engng*, 87, (2011), 15 – 47.

Cahn, J. W.; Hilliard, J. E.: Free energy of a nonuniform system. i. interfacial free energ. *J. Chem. Phys.*, 28, (1957), 258 – 267.

Cahn, J. W.; Hilliard, J. E.: Free energy of a nonuniform system. iii. nucleation in a two-component incompressible fluid. *J. Chem. Phys.*, 31, (1959), 688 – 699.

Cahn, J. W.; Hilliard, J. E.: On spinodal decomposition. *Acta Metall.*, 9, (1961), 795 – 801.

Di Leo, C. V.; Rejovitzky, E.; Anand, L.: A cahn-hilliard-type phase-field theory for species diffusion coupled with large elastic deformations: Application to phase-separating li-ion electrode materials. *J. Mech. Phys. Solids*, 70, (2014), 1 – 29.

Duda, F. P.; Souza, A. C.; Fried, E.: A theory for species migration in a finitely strained solid with application to polymer network swelling. *J. Mech. Phys. Solids*, 58, (2010), 515 – 529.

Friberg, O.: Jacobian matrices using the newmark direct integration scheme. *Comput. Struct.*, 25, (1987), 307 – 310.

Gómez, H.; Calo, V. M.; Bazilevs, Y.; Hughes, T. J. R.: Isogeometric analysis of the cahnhilliard phase-field model. *Comput. Methods Appl. Mech. Engrg.*, 197, (2008), 4333 – 4352.

Han, C. C.; Yao, Y.; Zhang, R.; Hobbie, E. K.: Effect of shear flow on multi-component polymer mixtures. *Polymer*, 47, (2006), 3271 – 3286.

Hong, W.; Wang, X.: A phase-field model for systems with coupled large deformation and mass transport. *J. Mech. Phys. Solids*, 61, (2013), 1281 – 1294.

Ju, L.; Zhang, J.; Du, Q.: Fast and accurate algorithms for simulating coarsening dynamics of cahnhilliard equations. *Comp. Mater. Sci*, 108, (2015), 272 – 282.

Kaessmair, S.; Steinmann, P.: Comparative computational analysis of the cahn hilliard equation with emphasis on c_1-continuous methods. *J. Comput. Phys.*, 322, (2016), 783 – 803.

Kästner, M.; Metsch, P.; d. Borst, R.: Isogeometric analysis of the cahnhilliard equation - a convergence study. *J. Comput. Phys.*, 305, (2016), 360 – 371.

Kuhl, E.; Schmid, D. W.: Computational modeling of mineral unmixing and growth. *Comput. Mech.*, 39, (2007), 439 – 451.

Lee, D.; Huh, J.-Y.; Jeong, D.; Shin, J.; Yun, A.; Kim, J.: Physical, mathematical, and numerical derivations of the cahnhilliard equation. *Comp. Mater. Sci*, 81, (2014), 216 – 225.

Liu, J.; Ded, L.; Evans, J. A.; Borden, M. J.; Hughes, T. J. R.: Isogeometric analysis of the advective cahnhilliard equation: Spinodal decomposition under shear flow. *J. Comput. Phys.*, 242, (2013), 321 – 350.

Taylor, R. L.: FEAP - finite element analysis program. http://projects.ce.berkeley.edu/feap (2014).

Ubachs, R. J. M.; Schreurs, P. J. G.; Geers, M. G. D.: Microstructure evolution of tinlead solder. *IEEE T. Compon. Pack. T.*, 27, (2004), 635 – 642.

Ubachs, R. J. M.; Schreurs, P. J. G.; Geers, M. G. D.: Phase field dependent viscoplastic behaviour of solder alloys. *Int. J. Solids Struct.*, 42, (2005), 2533 – 2558.

Wasylkiewicz, S. K.; Sridhar, L. N.; Doherty, M. F.; Malone, M. F.: Global stability analysis and calculation of liquid-liquid equilibrium in multicomponent mixtures. *Ind. Eng. Chem. Res.*, 35, (1996), 1395 – 1408.

Wells, G. N.; Kuhl, E.; Garikipati, K.: A discontinuous galerkin method for the cahnhilliard equation. *J. Comput. Phys.*, 218, (2006), 860 – 877.

Yeon, D.-H.; Cha, P.-R.; Kim, J.-H.; Grant, M.; Yoon, J.-K.: A phase field model for phase transformation in an elastically stressed binary alloy. *Modelling Simul. Mater. Sci. Eng.*, 13, (2005), 299 – 319.

Zao, Y.; Xu, B.-X.; Stein, P.; Gross, D.: Phase-field study of electrochemical reactions at exterior and interior interfaces in li-ion battery electrode particles. *Comput. Methods Appl. Mech. Engrg.*, 312, (2016), 428 – 446.

Zhu, J.; Lu, X.; Balieu, R.; Kringos, N.: Modelling and numerical simulation of phase separation in polymer modified bitumen by phase-field method. *Mater. Des.*, 107, (2016), 322 – 332.

Address:
Jannik Voges, Resam Makvandi, Daniel Juhre
Institut für Mechanik
Otto-von-Guericke-Universität Magdeburg
Universitätsplatz 2
D-39106 Magdeburg
email: `jannik.voges@ovgu.de`